Journal of the Brazilian Society of Mechanical Sciences and Engineering (2022) 44: 442
https://doi.org/10.1007/s40430-022-03754-x

TECHNICAL PAPER

Energy optimization of a centrifugal compressor along with wedge diffuser using ANN-coupled CFD

M. A. Hassan[1] · **Karteek Tamma Reddy**[1]

Received: 8 August 2021 / Accepted: 20 August 2022 / Published online: 4 September 2022

Abstract

The performance of a centrifugal compressor depends on multiple parameters, and optimization of these may lead to superior designs with improved efficiencies and energy savings. Impeller plays a vital role in compressor performance; hence, its optimization is performed to increase the efficiency. The parameters that affect the shape are considered in developing a parametric model. The computational fluid dynamics (CFD) screening test for the parametric model is performed using FINE™/Design3D. A database containing a few possible samples along with their CFD results is generated for training the model. Latinized Centroidal Voronoi Tessellations (LCVT) algorithm is used for the generation of samples in the predefined design space. With the generated database, the training of the optimization algorithm is carried out and the objective function along with required constraints is defined. The optimized design performance is tested and compared with the baseline design to judge the robustness of the algorithm.

Keywords Surrogate-assisted Optimization · Parametric model · NUMECA · Centrifugal compressor · ANN

Abbreviations

h	Static head developed, m
h_i, h_e	Specific enthalpy at inlet and outlet, J/kg
V^2	Tangential velocity of the impeller wheel or tip speed, m/s
z_i, z_e	Height above a reference line in gravitational force field at inlet and outlet, m
g	Acceleration due to gravity, m/s^2
T_i, T_e	Temperatures at inlet and outlet, K
ρ	Density of working gas, kg/m^3
V_i, V_e	Velocity of gas at inlet and outlet, m/s
ΔP	Difference in pressure, Pa
P_i, P_e	Total pressure at inlet and outlet, Pa
m	Mass flow rate, kg/s
η_{pol}	Polytropic efficiency
Q	Heat transfer rate, W
γ	Ratio of specific heats for working gas.
W_c	Work input, W
n	Polytropic index

Technical Editor: André Cavalieri.

✉ M. A. Hassan
hassan.me@nitjsr.ac.in

[1] Department of Mechanical Engineering, National Institute of Technology Jamshedpur, Jharkhand 831014, India

1 Introduction

The design and optimization of the turbomachinery by employing artificial intelligence have become a prevailing technique in industries from many decades. The centrifugal compressor in an automotive turbocharger is required to have a high pressure ratio, high efficiency, and, in particular, wide operating range. For a given compressor, the performance majorly depends on the impeller design. An optimized impeller design not only brings up the impeller performance but also delivers a more uniform flow to the diffuser and return channel thereby improving the performance of the given compressor stage. This attracted a significant number of researchers and developers to concentrate on optimizing the impeller over several decades.

Three-dimensional Reynolds-averaged Navier–Stokes equations (RANS) is being utilized to analyze the flow in turbomachinery over the last couple of decades [1, 2]. The inclusion of optimization methods along with the 3D-RANS reduces the computation cost in the design cycle of turbomachinery. In recent studies, various optimization techniques based on 3D RANS simulation have been applied for turbomachinery blade optimization by Trigg et al. [3]. Wahba and Tourlidakis [4] used a genetic algorithm to develop blade profiles for centrifugal impellers. An artificial neural network coupled with a Navier–Stokes solver is

developed by Pierret and Braembussche [5] for designing a turbomachinery blade. Using Navier–Stokes analysis Ahn and Kim [6] optimized a compressor rotor in 2003. Jang and Kim [7] employed the response surface method (RSM) to optimize a stator blade in a transonic axial compressor. The thickness and stacking distribution of a compressor blade is optimized using surrogate model by Samad and Kim [8]. Bonaiuti et al. [9] used the design of experiments technique (DoE) to optimize an impeller of a transonic centrifugal compressor. He has chosen the meridional contour along with the angle of the impeller as the design variables for the optimization. Bonaiuti and Pediroda [10] utilized a genetic algorithm to optimize an industrial centrifugal compressor. Cosentino et al. [11] optimized a 3D impeller which is described by 15 parameters using genetic algorithm which has been coupled with the artificial neural network (ANN).

Making an impeller geometry using Bezier curves makes the curvatures smooth and improves the performance of the compressor. Several researchers have been focusing on the optimization of the impeller blade described by Bezier curves. Benini [12] used these Bezier curves which are controlled by Bezier poles for the construction of blades during multi-objective optimization considering efficiency and pressure ratio as objectives. In a view to assisting the researchers in the optimization of turbomachinery, several neural networks are considered during product development.

Optimization of turbomachinery utilizing radial basis neural network (RBNN) is being used by many researchers. Optimization based on RBNN has been performed by Huppertz et al. [13]. Coupling this RBNN with the response surface method built with a lower-order polynomial has shown a good result in the research performed by Rai and Madyavan [14]. Applications of the artificial neural network in industries have been extensively reviewed by Meireles et al. [15] in 2003.

In this work, a single-stage centrifugal compressor is considered for optimization which is shown in Fig. 1. A comparison with the baseline model has been carried out to obtain an improved design. This baseline model is a typical high-speed single-stage centrifugal compressor. A tuned radial basis function neural network coupled with CFD code has been employed for this optimization. NUMECA (a commercial software) along with MINAMO (a commercial optimization tool) has developed a tool where users can develop and improve the algorithm which is responsible for the optimization of turbomachinery. This tool has a specialty where the predicted design undergoes a CFD analysis and the result obtained is verified for meeting the predefined criteria. If it fails to meet the criteria, this proposed sample will be added to the existing database and again the algorithm is trained for the next proposal. This loop continues until the criterion is reached. This process of correcting the database refines the response surface near to optimum making it more accurate for prediction.

Figure 1 represents the meridional view of an impeller along with the wedge diffuser. In this work, we have optimized both the impeller and diffuser. The main objective of this optimization is to increase the efficiency of the compressor by meeting the required pressure ratio criteria. The major constraint in this optimization is to keep the work coefficient same as that of baseline.

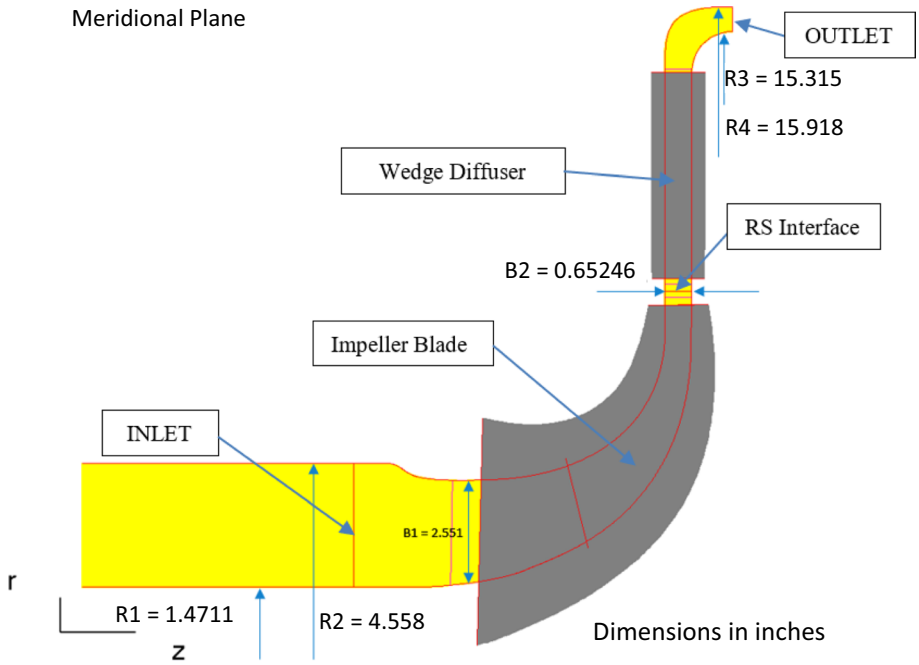

Fig. 1 Compressor stage considered for optimization

2 Mathematical modeling

By applying energy balance to the compressor, the obtained steady flow energy equation is given as follows:

$$m\left(h_i + \frac{V_i^2}{2} + gz_i\right) - Q = m\left(h_e + \frac{V_e^2}{2} + gz_e\right) - W_c \quad (1)$$

It is well known that the radial pressure gradient is controlled by the main flow and the distinction between inlet velocity and exit velocity magnitude is too small. The variations in kinetic energy and potential energy are negligible; hence, the above equation can be reduced to:

$$mh_i - Q = mh_e - W_c \quad (2)$$

In general, the heat transfer rate Q in a centrifugal compressor is generally negligible (as the available area for heat transfer is small) when compared to other energy terms, so the adiabatic work input of a centrifugal compressor is given by:

$$W_c = m\left(h_e - h_i\right) \quad (3)$$

The above equation is valid for both reversible and irreversible adiabatic processes, provided that in the case of irreversible compression processes, actual enthalpy is used at the exit. During reversible adiabatic compression, the input work required for compression is given by:

$$W_{c,isen} = m\left(h_e - h_i\right)_{isen} \quad (4)$$

Then using the thermodynamic relation, $(Tds = dh - vdp)$ and $PV^{\gamma} = K$ the isentropic work of the compressor is given by:

$$W_{c,isen} = \frac{\left(\frac{P_e}{P_i}\right)^{\frac{\gamma-1}{\gamma}} - 1}{\frac{T_e}{T_i} - 1} \quad (5)$$

To account for the irreversibility's in centrifugal compressors, a polytropic efficiency η_{pol} is defined and is given by:

$$\eta_{pol} = \left(\frac{n}{n-1}\right)\left(\frac{\gamma-1}{\gamma}\right) \quad (6)$$

We know for polytropic process $PV^n = Con$. From this, we can obtain the temperature ratio as

$$\frac{T_e}{T_i} = \left(\frac{P_e}{P_i}\right)^{\frac{n-1}{n}} \quad (7)$$

And by substituting Eq. 6 in 7, we can obtain the temperature ratios in terms of polytropic efficiency as follws:

$$\frac{T_e}{T_i} = \left(\frac{P_e}{P_i}\right)^{\frac{n-1}{n}} = \left(\frac{P_e}{P_i}\right)^{\left(\frac{\gamma-1}{\gamma}\right)\left(\frac{1}{\eta_{pol}}\right)} \quad (8)$$

Applying natural log and resolving it further, we can obtain the polytropic efficiency as given in Eq. (9).

$$\eta_{pol} = \left(\frac{\gamma-1}{\gamma}\right)\frac{\ln\left(\frac{P_e}{P_i}\right)}{\ln\left(\frac{T_e}{T_i}\right)} \quad (9)$$

Details of Eqs. (1–9) can be found elsewhere [1]. One can observe from Eq. (9) that isentropic efficiency depends upon the outlet and inlet conditions of a particular compressor. This makes it not viable to differentiate the compressors using isentropic efficiency. To eliminate this, polytropic efficiency is considered where the efficiency depends only on the path of compression described as Eq. (9). Irrespective of the outlet conditions, a compressor is said to have a fixed polytropic efficiency.

2.1 Computational modeling

Time-dependent Reynolds-averaged Navier–stokes equations are solved using the finite volume method in NUMECA's Fine™/Turbo. A second-order central scheme with second- and fourth-order artificial dissipations is adopted for spatial discretization. Time marching is performed with an explicit four-stage Runge–Kutta scheme, coupled with local time-stepping and implicit residual smoothing technologies. Turbulence is modeled using SST (shear stress transport) extended wall function turbulence model [2, 6]. The extended wall function is an alternative and widely employed approach to model the near-wall region. Extended wall functions use empirical laws to circumvent the inability model to predict a logarithmic velocity profile near a wall.

A structured multi-block mesh with 2,609,739 nodes has been generated for a single blade passage with periodic boundaries in a pitch-wise direction using NUMECA's Autogrid. Figure 2 shows the blade to blade view of structured mesh generated in Autogrid. The first cell height is specified in such a way that the y + at all the solid surfaces stays below 5. The pressure inlet and mass flow outlet boundary conditions are specified in the CFD solver. The compressor is designed to have a mass flow of 4.39 kg/s of air.

A full multigrid strategy has been employed for achieving faster convergence reducing the computational cost [2, 12]. In multigrid strategy, the RANS equations are first solved on the coarser grid level and the converged solution is then interpolated onto the finest grid level. This helps in providing a good initial solution for the finest grid level. The number of intermediate grid levels depends upon the

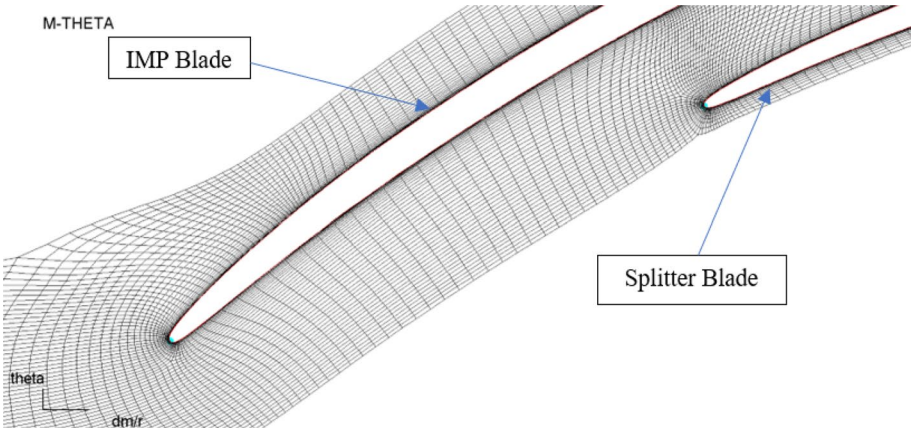

Fig. 2 B2B mesh of the impeller at 50% span

Table 1 Mesh dependency study

	M1	M2	M3	M4	M5
No. of Nodes	1,024,315	1,435,679	2,018,526	2,609,739	3,152,368
Dp_Efficiency (η_{pol})	88.1255	87.19613	86.5219	86.49385	86.48312
$\Delta\ \eta_{pol}$	-	0.92937	0.67423	0.02805	0.01073
$\%\ \Delta\eta_{pol}$	-	1.054598	0.773234	0.03242	0.012406

mesh size in i, j and k directions. The convergence criteria were established when normalized residuals were less than 1.3×10^{-5} and 5×10^{-7} for Samad and Kim [8] and Benini [12], respectively. Accordingly, for the current work, the convergence criteria for global residual are set to 10^{-6}. Further drop in residuals was having no effect except increase in the computation time. Before this, mesh dependency study has been performed in order to achieve an optimal mesh. The results obtained during this study are tabulated in Table 1. The names M1, M2, M3, M4 and M5 are used to denote different grids where the resolution of the grid increases from M1 to M5, and the same can be observed in node count.

From Table 1, it is clear that there is no noticeable change in design point efficiency from mesh M4 to M5. With this, mesh M4 is considered as optimal mesh and further analysis has been carried out using the M4 mesh template. They were tested for all different configurations that have been simulated in the study.

Figures 3 and 4 show the hexahedral multi-block structured mesh generated using the optimal mesh template. All the simulations including the database generation and optimization are carried out using this mesh template.

2.2 Optimization

The procedure for optimization is shown in Fig. 5 where you can observe that optimization starts with parametric model generation, in which the considered geometry is parameterized for optimization. After the parametrization, a screening

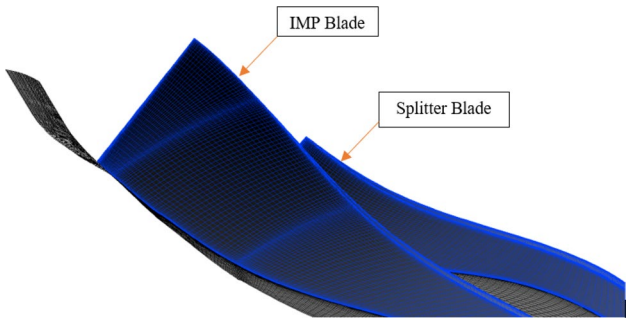

Fig. 3 Hexahedral multi-block structured mesh of the impeller

CFD simulation is done to compare the results of the parametric model with the baseline geometry.

Next to the parametrization, it is database generation where a few numbers of possible designs within the design space are analyzed in CFD software (FINE™ Turbo 14.1) and the obtained results are stored in a database. With this database, the selected surrogate model is trained and used for optimization. The proposed design then undergoes a CFD analysis where the results obtained are verified for meeting the predefined criteria. Once the proposed model meets the design criteria, the algorithm stops the optimization process and proposes the final optimal design. If in case the proposed model fails to meet the design criteria, it is then added to the existing database and training is repeated once again with the new database. This loop goes on until the specified criteria are reached or the specified number of optimization iterations completes.

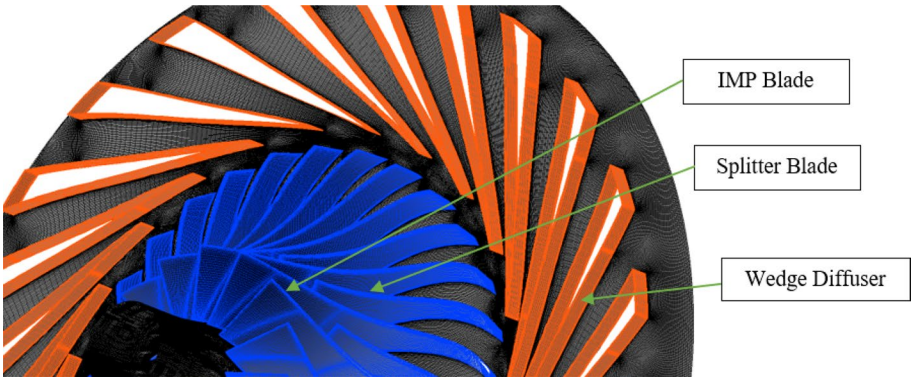

Fig. 4 Hexahedral multi-block structured mesh of complete stage

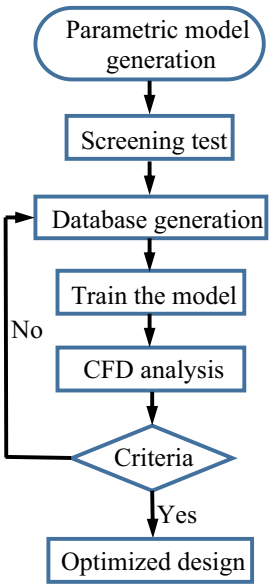

Fig. 5 Optimization procedure

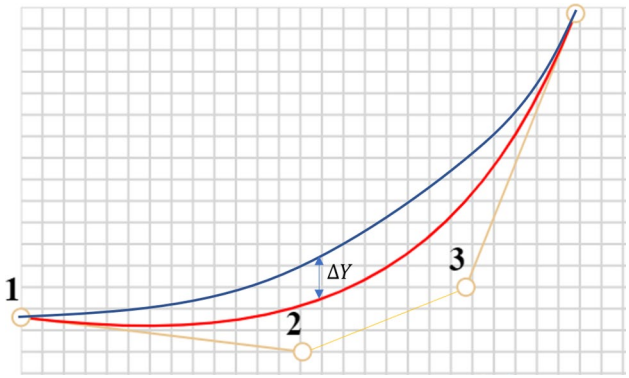

Fig. 6 Fitting of Bezier curve

Before the database generation, the geometry needs to be parameterized. In this case, NUMECA's AutoBlade is used to parametrize the existing compressor design allowing us to grab on easy control of impeller design changes. An iterative fitting process is done to get the best fit of the parametric model. The working fluid for compression is considered as air, and the corresponding mass flow rate at the design point is considered 4.39 kg/s; also, the impeller is rotating at 21,789 RPM. The CFD simulation is performed with pressure inlet and mass flow outlet boundary conditions with a CFL = 3.

2.3 Parametric model generation

To generate the parametric model of the baseline geometry, a set of Bezier curves are fitted along the flow path and to the beta and thickness profiles. An iterative fitting process is employed to get the best fit to the baseline model by using Bezier curves. Figure 6 gives a clearer impression of the fitting process. The blue curve in Fig. 6 represents the original compressor design whereas the Bezier curve attempted to fit is represented by red.

The position of poles 2 and 3 is updated in an iterative process such that the error ΔY between the original curve and the Bezier curve is reduced. The fitting is carried out by employing the least square method where the square of the error between the two curves is minimized. The equation for the Cubic Bezier curve is as follows [18]:

$$x(t) = (1-t)^3 x_1 + 3(1-t)^2 t x_2 + 3(1-t) t^2 x_3 + t^3 x_4 \quad (10)$$

$$\left(y(t) = (1-t)^3 y_1 + 3(1-t)^2 t y_2 + 3(1-t) t^2 y_3 + t^3 y_4\right) \quad (11)$$

where $t \in [0, 1]$

The fitting process is repeated several times until a close match to the baseline geometry is obtained. From Fig. 7, one can observe the fitting of Bezier curves to the hub curve to parametrize the model. The obtained parametric model is then analyzed with the help of fine turbo (CFD solver), and the results obtained are then compared with the baseline results. Once the results obtained from the screening test meets the satisfactory limits, then the developed parametric model is then passed on to database generation. Before passing the parametric model to the database generation, the range for the parameters that are

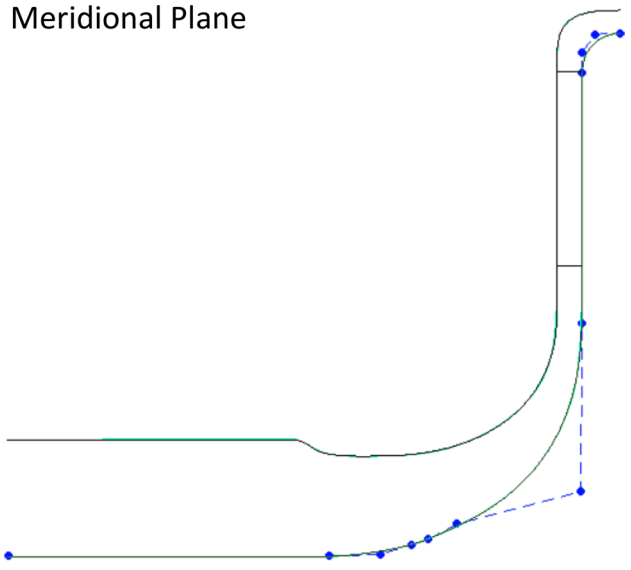

Fig. 7 Bezier curve fitting to Hub curve

to be optimized is specified in the AutoBlade environment itself.

2.4 Database generation

Before building a surrogate model either for optimization or statistical analysis purposes (e.g., ANOVA; analysis of variance), a set of sample points that uniformly covers the parametric design space must be generated to train the neural network. CFD analysis will be carried out for the generated sample points to obtain the function responses. Flowchart shown in Fig. 8 describes the process of database generation.

For building a robust surrogate model, the design of experiment (DoE) plays an important role. DoE should be generated in such a way that the entire design space should be covered with sample points so that the built surrogate model can capture the entire design space. For the generation of DoE, we have few algorithms which are discussed here.

From Fig. 9, we can observe that out of all the available models, Latinized Centroidal Voronoi Tessellations (LCVT) with 100 samples covers the given parametric design space more uniformly than the other available models. In the present work, LCVT algorithm is used to fill up the parametric design space. Once the samples are placed in the parametric design space, each sample then undergoes a CFD computation parallelly depending on available resources and the responses of all the defined quantities are computed.

Table 2 contains the quantities that are evaluated during the database generation for the optimization procedure. A total of 30 sample points is generated using six design variables to build the surrogate model. The quantities evaluated during the database generation are listed in Table 2. Dp, Sp and Cp stand for design point, surge point and choke point, respectively.

2.5 Optimization methodology

The optimization of the impeller stage is carried out with the help of a surrogate-assisted algorithm. Surrogate-based optimization (SBO) mainly utilizes surrogates or approximations instead of expensive high-fidelity CFD analysis results to reduce the computational time required and maintain it within affordable limits [16, 17]. However, the performance of this surrogate-assisted optimization majorly depends on the following key elements:

1. The surrogate model.
2. The underlying optimization algorithm.
3. The training (design of experiments and infill criteria).
4. The surrogate model management schemes.

A typical surrogate-based design optimization cycle is shown in Fig. 10.

The main challenge in surrogate-assisted optimization is to build a surrogate model that will be as accurate as possible by utilizing as few expensive high-fidelity CFD evaluations as possible. For most simple cases, the surrogate model is developed using polynomial fitting surfaces. In general, for high dimensional and highly multimodal problems, polynomial fitting surfaces are not applicable. In such cases, various nonlinear data-fitting models are employed to build the surrogate model such as radial basis functions networks

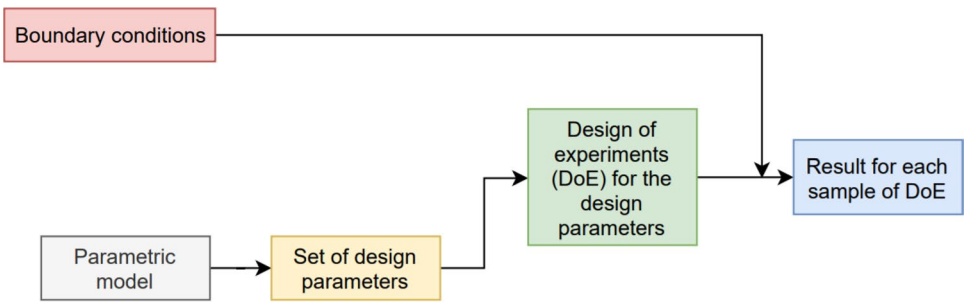

Fig. 8 Database generation flowchart

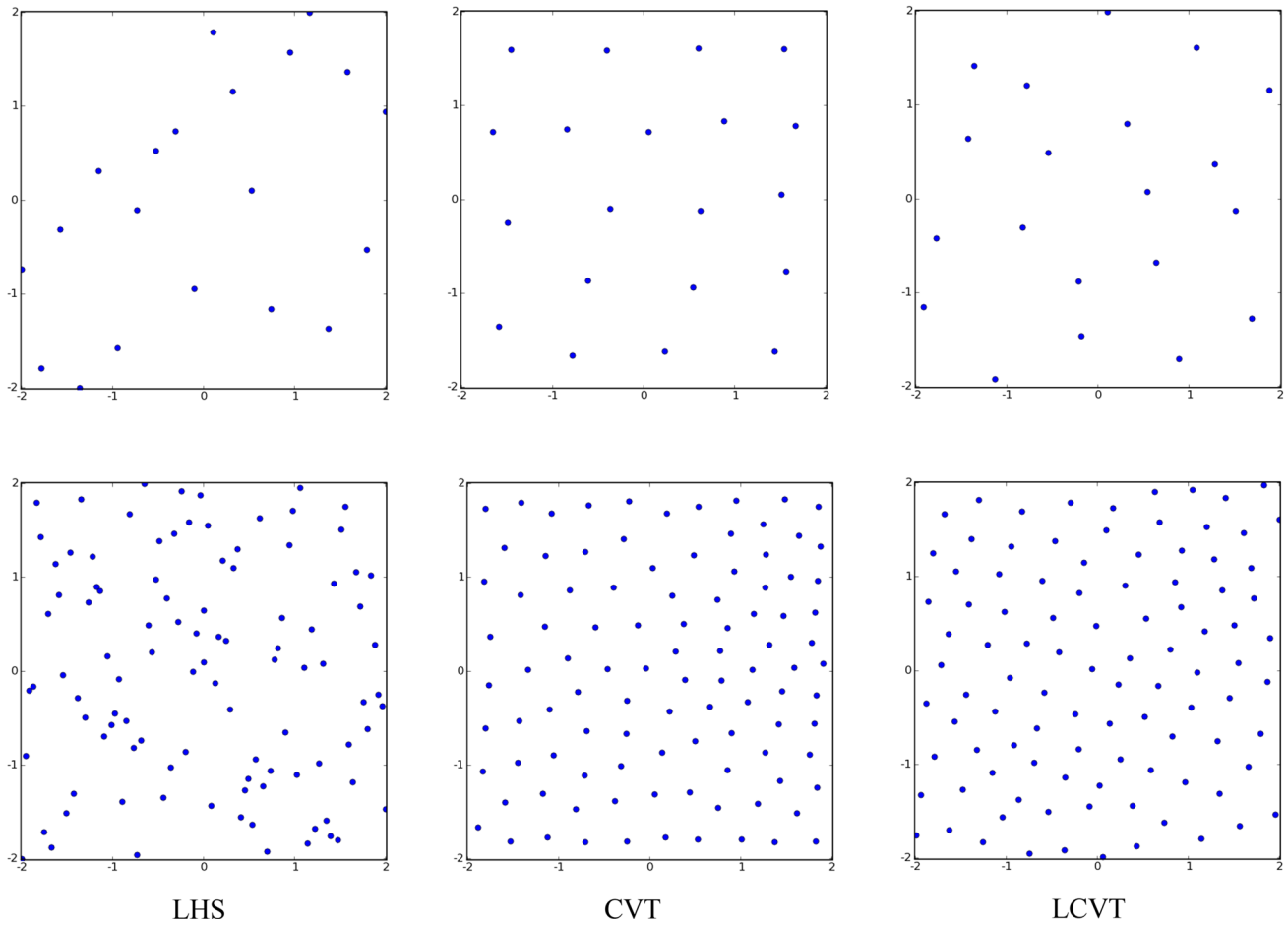

Fig. 9 DoE Placement-LHS, CVT, LCVT-top (20samples), bottom (100 samples)

Table 2 Quantities Evaluated during database generation

S. No	Quantity
1	Polytropic efficiency (Dp, Sp, Cp)
2	Isentropic efficiency (Dp, Sp, Cp)
3	Convergence (Dp, Sp, Cp)
4	Pressure Ratio (Dp, Sp, Cp)
5	Work Coefficient offset (Dp, Sp, Cp)
6	Delta Theta (sections- 12, 23, 34, 45,51)

(RBFN), support vector regression, Kriging and artificial neural networks. Unlike polynomial fitting surfaces, these nonlinear models are capable of decoupling the free parameters from the respective design parameters. This technique makes these models more robust in highly nonlinear cases. For this optimization tuned radial basis functions network (TRBFN) is used to develop the surrogate model. The equation for the TRBFN model is expressed as follows [18]:

$$y(x) = \sum_{i=1}^{n} w_i h\left(x - c_i, \sigma_i\right) \tag{12}$$

where.

1. y is the model defined as a combination of n radial basis functions.
2. h is a basis function or hidden unit function.
3. w_i's denotes the weights of n radial basis functions.
4. c_i's and σ_i's denotes the centers and widths of the basis function.
5. σ is a parameter which controls the interpolation smoothness.

Our goal is to find out the weights w_i of each radial basis function specified in Eq. (12). Weights w_i are chosen in such a way that the error between the real outputs and predicted outputs is minimized. The basis functions used are expressed in Table 3.

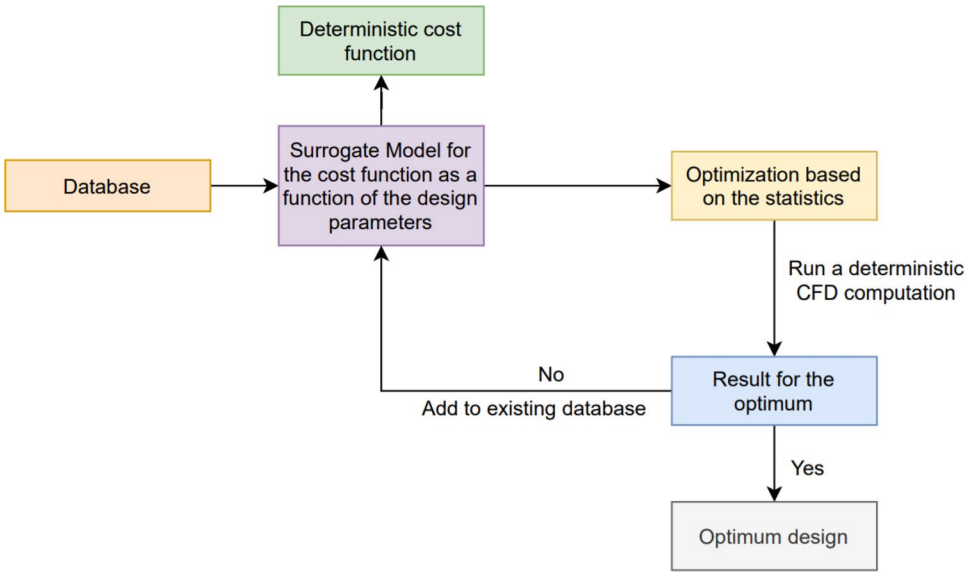

Fig. 10 Surrogate-based optimization design cycle

Table 3 Basis Functions

Name	Expression of $h(r, \sigma)$
Gaussian	$exp\left(-\frac{r^2}{2\sigma^2}\right)$
Multiquadric	$\sqrt{\frac{r^2}{\sigma^2}+1}$

Table 4 Validation analysis

Variable	R^2	R^2_{adj}
Work Coefficient	0.989	0.982
Static pressure ratio	0.998	0.990

The major difference between the two functions is that the Gaussian function decreases monotonically to the distance from a central point whereas the multiquadric one increases. The classical RBFN model uses the multiquadric function with a fixed σ_i for all i. The tuned RBFN model uses a tuning to generate the surrogate model without the need of user to specify the type of basis function and hyper-parameter values. It automatically switches between the Gaussian and multiquadric basis functions to achieve the best results. While training, the model uses a leave-one-out based heuristic to select the radial basis function h (Gaussian or multiquadric) and to adjust the parameters σ_i's for the experiment plan to obtain a higher quality model.

2.5.1 Validation

The reliability of the surrogate model is assessed through leave-one-out (LOO) cross-validation. The correlation coefficient R is calculated at each design iteration using this LOO cross-validation technique. This LOO cross-validation eliminates the need for external data set for validation; instead, it uses a single sample point from original data as a validation point, and the remaining sample points are used for training. This is repeated such that each sample point in the database is used once as the validation data. Finally, one obtains a set of estimated outputs (with LOO) and one of the real outputs for each response. These output sets can be statistically analyzed for error estimation. The correlation coefficient is computed and given by [18]

$$R = \frac{n\sum_{i=1}^{n} f_i y_i - \sum_{i=1}^{n} f_i \sum_{i=1}^{n} y_i}{\sqrt{n\sum_{i=1}^{n} f_i^2 - \left(\sum_{i=1}^{n} f_i\right)^2}\sqrt{n\sum_{i=1}^{n} y_i^2 - \left(\sum_{i=1}^{n} y_i\right)^2}} \tag{13}$$

where f_i and $y_i (i = 1, \ldots, n)$ denotes the real values and predicted values, respectively, for n sample points. R always takes a value between -1 and 1 and measures the degree to which two variables are linearly related. A value of R = 1.0 indicates a perfect fit. Once the surrogate model is generated, optimizer comes into the picture.

The validation of the model has been checked through the statistical analysis of R^2 and R^2_{adj} (R^2 adjusted to the number of parameters used in the model). A sensitivity analysis was also carried out to examine the effect of single parameters on the responses and the effect of their integration. The validation analysis is presented in Table 4. It can be observed that the magnitude of R^2 is very high for all cases and it indicates that the selection of mode is correct. The current model has been employed to replicate the results of Samad

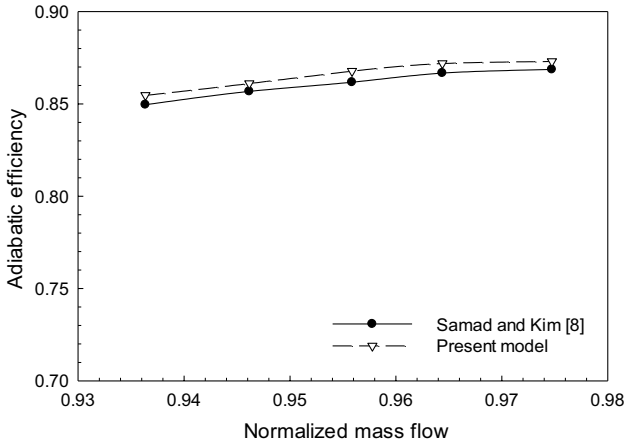

Fig. 11 Result validation with previous work [8]

and Kim [8]. The adiabatic efficiency obtained has been compared and is depicted in Fig. 11. A nice agreement has been observed with an average deviation of 0.6%.

Multi-objective surrogate-assisted evolutionary algorithm optimizer also known as multi-objective optimizer (MOO) is used to find the best optimal design. Most realistic optimization problems require the simultaneous optimization of more than one objective as in this particular case we need to maximize the polytropic efficiency, and at the same time, we need to minimize the convergence at the design point. These objectives ensure obtaining the design with a high level of convergence and improved performance. In MOO, there is no single best solution. So, the actual aim of this multi-objective optimization (MOO) is to find out a good compromised or balanced design instead of a single solution. Handling of constraints is the most complicated task in the Evolutionary algorithm. Penalization of the designs violating the constraints is the most common approach used to handle the constrained model. The major difficulty in this penalization process is calculating appropriate values for penalty parameters. In most cases, users are required to experiment with different penalty values to obtain the best results. In order to eliminate this problem, Deb's constraint tournament selection method is employed to handle the unfeasible solutions. This method performs a pairwise comparison between the designs eliminating the need of penalty parameters to drive the optimization process toward the feasible regions.

This technique has been demonstrated to be successful [19], especially in providing feasible solutions to highly constrained problems. But as a drawback, the optimizer might focus on local extrema too rapidly if the design space is scarcely populated; thus, it is strongly recommended to use a good number of design samples during database generation to cover the entire design space so that multiple extrema (if they exist) are well represented. This method always privileges feasible solutions and is generally more likely to converge toward a feasible solution. In order to deal with the simulation failures, i.e. (when the simulation software does not return any answer due to convergence problem, mesh generation problem due to unrealistic geometries, or insufficient convergence of the detailed simulation), the algorithm adds the penalties to the individuals which are close to the regions where the previous simulation has failed thereby driving the population toward the region with high numerical stability. With the generated database, the surrogate model is developed based on the TRBFN algorithm. Once the training is completed, a set of objective functions along with all the constraints are defined for optimization. Then, the optimizer begins its search for optimal design based on the defined constraints and objectives. The objective functions and constraints imposed for the optimization are presented in Table 5 and 6, respectively.

The goal of this optimization is to maximize the Polytropic efficiency at the design point while satisfying all the imposed constraints within the parametric design space. In this case, the primary constraint is to maintain the static pressure ratio as that of baseline so that the optimized geometry can deliver minimum required pressure ratios; along with this, the major constraint is to limit the working coefficient to that of a baseline so that existing work output surface will be sufficient enough to run the compressor. The static pressure ratio has a lower bound value of 4.2535.

Table 5 Objectives

S. No	Objective	Type	Weights
1	Dp Polytropic Efficiency	Maximize	100
2	Convergence	Minimize	2
3	Work Coefficient Offset (Design)	Minimize	10
4	Work Coefficient Offset (Surge)	Minimize	10
5	Work Coefficient Offset (Choke)	Minimize	10

Table 6 Constraints

S. No	Constraint	Bound	Value
1	Static pressure ratio	Lower bound	4.2535
2	Design convergence	Upper	0.2
3	Work coefficient offset (design)	Upper	0.05
4	Work coefficient offset (surge)	Upper	0.05
5	Work coefficient offset (choke)	Upper	0.05
5	Delta Theta_12	Upper	2
6	Delta Theta_23	Upper	1
7	Delta Theta_34	Upper	3
8	Delta Theta_45	Upper	1.6
9	Delta Theta_51	Upper	2

In a view to increasing the robustness of the algorithm, a move-limit strategy is applied. This strategy adjusts the range of design parameters during the optimization process and confines the optimization search to smaller regions in the design space thereby eliminating the unnecessary design space and making the optimization confined to a more useful area. This improves the accuracy of the surrogate model making the optimizer reach the optimal point with less number of design iterations. This improvement in accuracy and elimination of redundant design space due to narrowing of the optimization search leads to significant reduction in computational cost and cycle time [20, 21].

With all these settings, the optimization algorithm proposes the first optimum design along with the predicted outputs for the objective functions, this optimized design then undergoes a CFD analysis, and the results obtained are verified for meeting the predefined criteria. Once the proposed model meets the design criteria, the algorithm stops the optimization process and outputs the final optimal design. If in case the proposed model fails to meet the design criteria, it is then added to the existing database and training is repeated once again with the new database. This loop goes on until the specified criteria are obtained or the specified number of optimization iterations completes. This process of correcting the database refines the response surface near to optimum making it more accurate for prediction.

3 Results and discussion

Before starting the optimization process, the developed parametric model is verified with the given baseline geometry to verify the goodness of fit performed during parametric model generation. Figure 12 shows the performance comparison between the parametric model and the baseline geometry under the same set of operating and boundary conditions solved using NUMECA's Fine Turbo CFD solver. From Fig. 12, we can observe that the performance of the parametric model generated is very close to the baseline model. As the performance seems to be fine, the parametric model is then considered for optimization. It is worth remembering that both the models are meshed using the same mesh template M4 which is found as the optimal mesh during the mesh dependency study.

Figure 13 represents the variation of polytropic efficiency at the design point to optimization iterations. We can observe the improvement in efficiency at the design point as the optimization progresses. It is worth mentioning that the points represented in blue color corresponds to database and the points in orange color corresponds to optimization. As the optimization progresses, the response surface gets refined more at the optimal location. This makes the algorithm more accurate for prediction at the optimal location. The reference line present in Fig. 13 and Fig. 14 corresponds to baseline.

In this way, the algorithm tries to improve the efficiencies up to the possible extent within the parametric design space depending upon the set of constraints. After specified iterations, the algorithm reduces the search area in the design space and concentrates more on the optimal region. This improves the response surface and predictability of the surrogate model.

Figure 14 represents the variation of static pressure ratio at design point to optimization iterations. One can observe that the optimized sample has higher pressure ratio than the baseline. Due to this optimization, the pressure ratio at design point has been improved by 3.322%.

The performance comparison of the optimized sample (design 57) with the baseline geometry is shown in Fig. 15 along with two other best samples (design 59 and 61). It

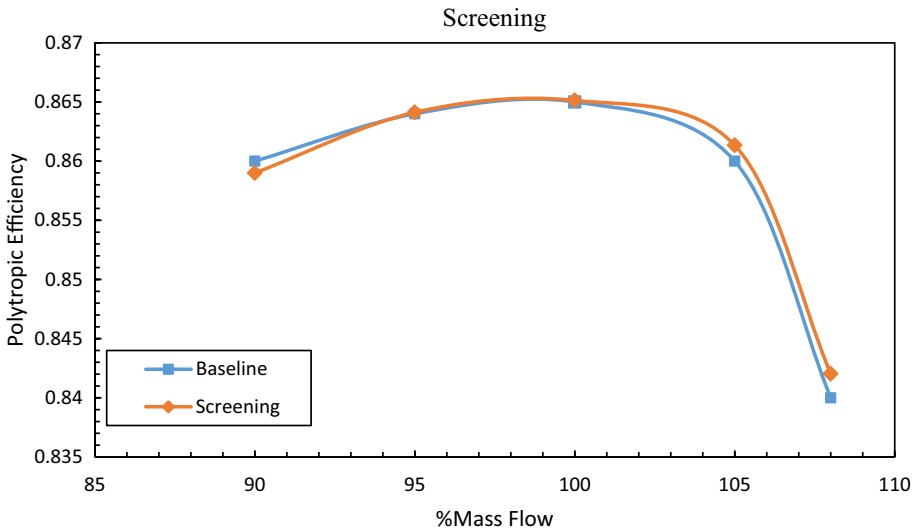

Fig. 12 Performance of baseline and parametric models

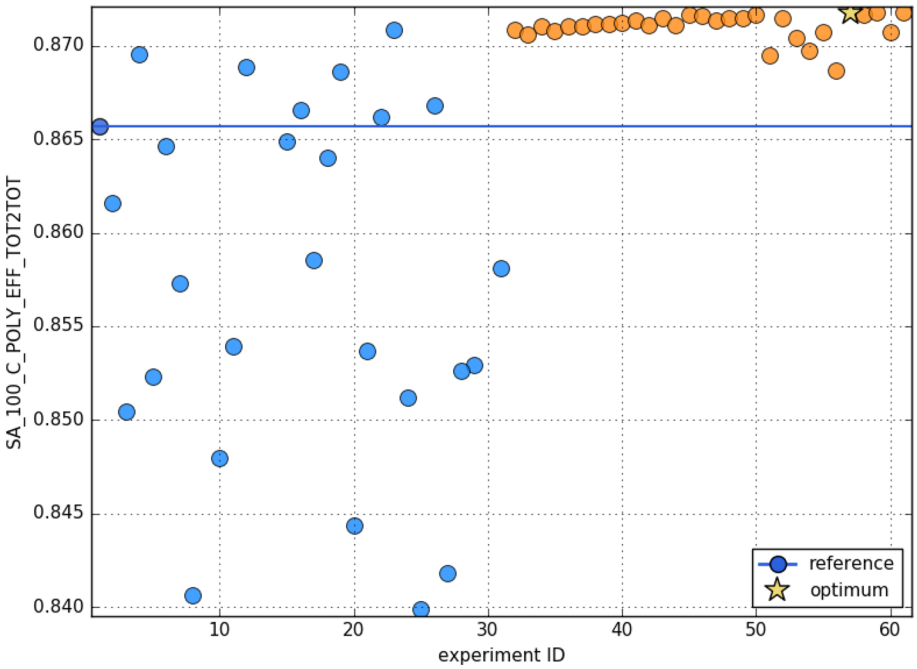

Fig. 13 Variation of polytropic efficiency (Design point) on Y-axis with respect to experiment ID

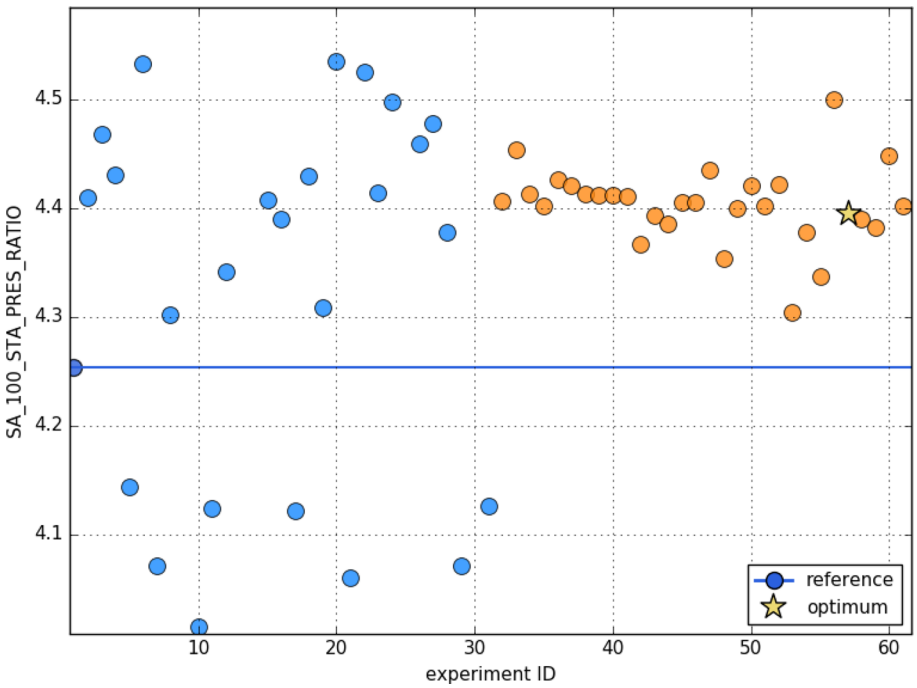

Fig. 14 Variation of static pressure ratio (Design point) on Y-axis with respect to experiment ID

can be observed that design 57 performance is superior to the baseline. We can see a significant amount of increase in performance throughout its operating range. Choke performance has improved well when compared to other operating points. Similar trend can be observed in Fig. 16 where the static pressure ratio has improved well at the choke point when compared to other points. The best three designs from the optimized samples are considered for further analysis. These three designs are mechanically analyzed, and finally, one optimal design is suggested for the particular family.

Variation of the pressure ratio for the baseline and optimum sample (design 57) with respect to mass flow rate is shown in Fig. 16. The increase in pressure ratio for the optimum sample with comparison to baseline has been observed. This says that the optimized geometry will be reaching high pressure ratios than the baseline. Also, from Fig. 17 by observing the work coefficient graphs, we can ensure that

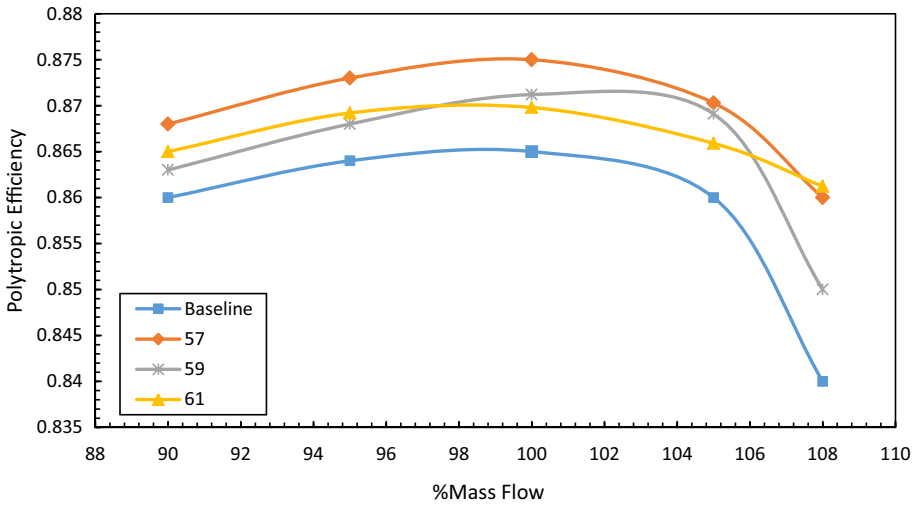

Fig. 15 Performance of baseline and optimum model (design 57)

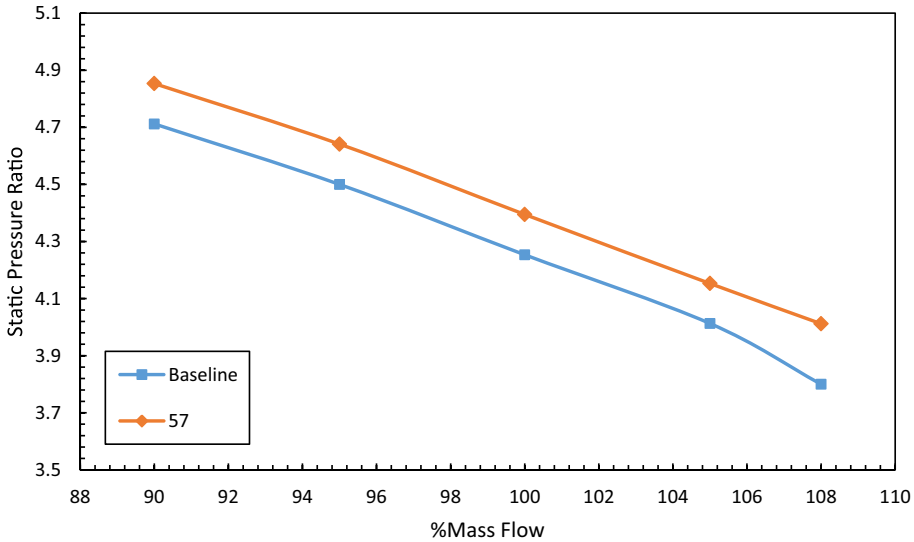

Fig. 16 Variation of pressure ratio of baseline and design 57 with respect to mass flow rate

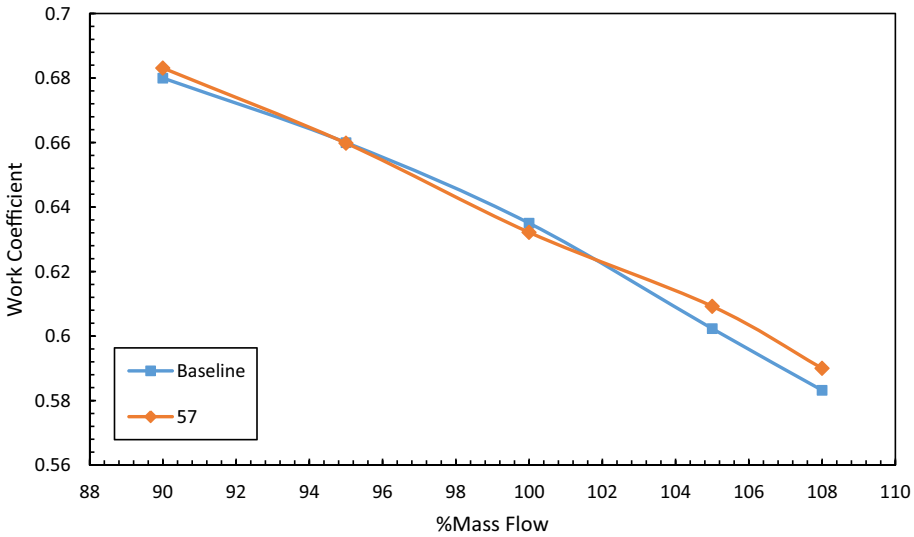

Fig. 17 Variation of work coefficient of baseline and design 57 with respect to mass flow rate

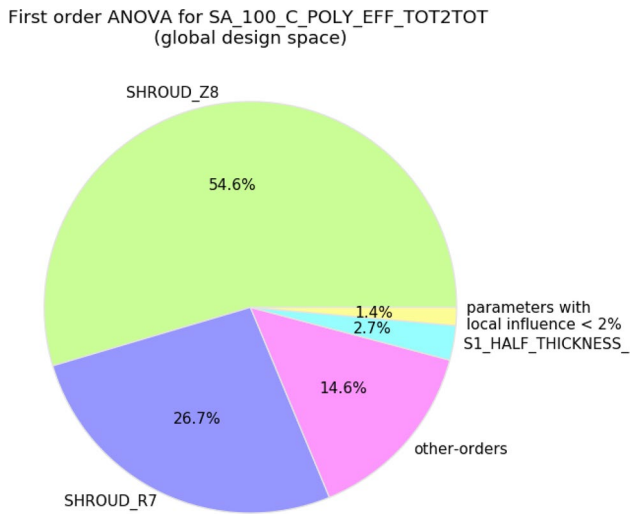

Fig. 18 Parametric influence on polytropic efficiency

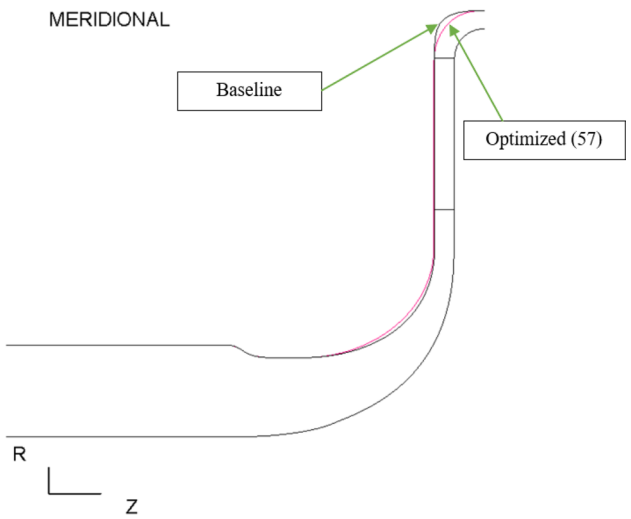

Fig. 19 Optimized sample hub and shroud comparison

the optimized sample will be consuming same work input as that of baseline. In addition to these plots, we can have a look at the parametric influence on the global objective that is defined during optimization. Figure 18 containing the pie chart represents the influence of different geometrical parameters on polytropic efficiency.

This parametric influence chart gives us a good insight for developing a new compressor design for the same family. From Fig. 18, we can notice that Shroud_Z8 has a greater influence on polytropic efficiency. With the help of this parametric influence chart, we can concentrate more on that particular set of parameters while designing a compressor stage of the same family.

To obtain a clear idea in terms of performance improvement, the percentage increase in the efficiencies at all 3 operating points, i.e., design point, chokepoint and surge point for the optimized design is tabulated in Table 7.

From Table 7, it can be noticed that the optimum sample (design 57) has an increase in efficiency of 1.15% at the design point, 0.93% at the surge point, and 2.33% at the choke point. During the optimization, it is observed that the increase in polytropic efficiency is majorly limited due to the tip gap present in the impeller that is contributing to major mixing losses. Unfortunately, we are not able to reduce the tip gap due to the creep occurring in the impeller as it is spinning at higher rotation speeds.

Table 7 Performance of optimal design

Exp. ID	Baseline	Optimum (57)	% increase
Surge	0.86	0.868	0.930233
Design	0.865	0.875	1.156069
Choke	0.84	0.859618	2.335476

The changes that occurred in hub and shroud curvature for the optimized sample are shown in Fig. 19. The pink one represents the optimized geometry, and the white one represents the baseline. From the figure, it is clear that shroud curvature at the existing bend has been improved for optimum design. Figure 20 depicts the static pressure contours of both baseline and optimized design. One can observe that the optimized sample is having a good rise in static pressure than that of the baseline. Along with these, the contours of velocity magnitude at the L bend are shown in Fig. 21. One can observe that the flow is much more uniform in the optimized sample.

A comparison of the absolute Mach number contour for the optimized sample (design 57) and the baseline is shown in Fig. 22. We can observe the reduction in disturbance induced at the blade leading edge for both the main blade and the splitter blade. Figure 23 represents the pictorial view of the optimized impeller.

4 Conclusion

The optimization of the given centrifugal compressor is performed by NUMECA, and the results obtained are discussed. A total of six parameters are optimized to get a geometry with an increase in polytropic efficiency of 1.15% at the design point, 0.93% at the surge point, and 2.33% at the choke point. In this optimization, constraints are applied in such a way that optimized geometry will be having a pressure ratio greater than that of the baseline with the same work consumption. Pressure contours are also presented. During the optimization, it is observed that the performance of the compressor is limited due to the tip gap present in the impeller which is contributing to major mixing

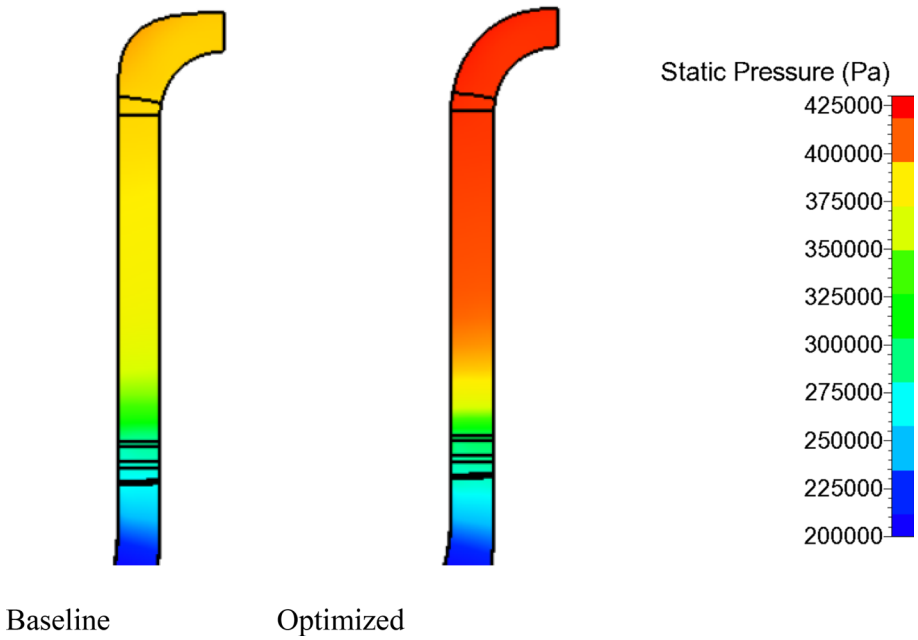

Fig. 20 Static pressure contours of both baseline and optimized geometry at diffuser

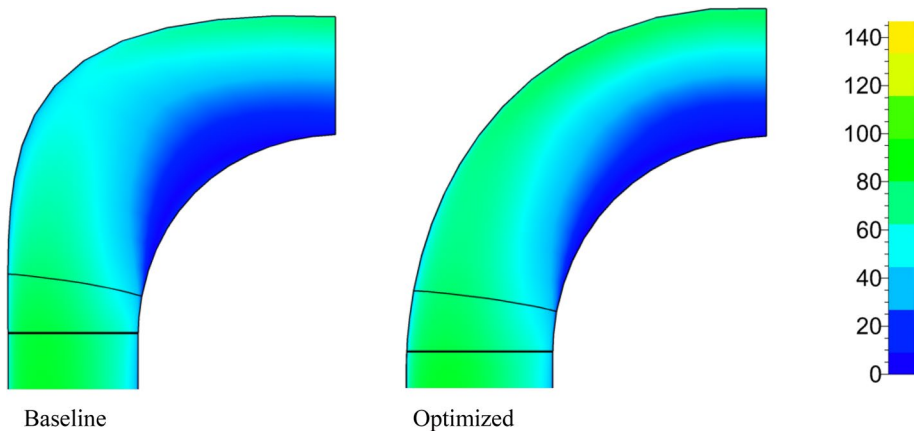

Fig. 21 Velocity contours (m/s) of both baseline and optimized geometry at L bend

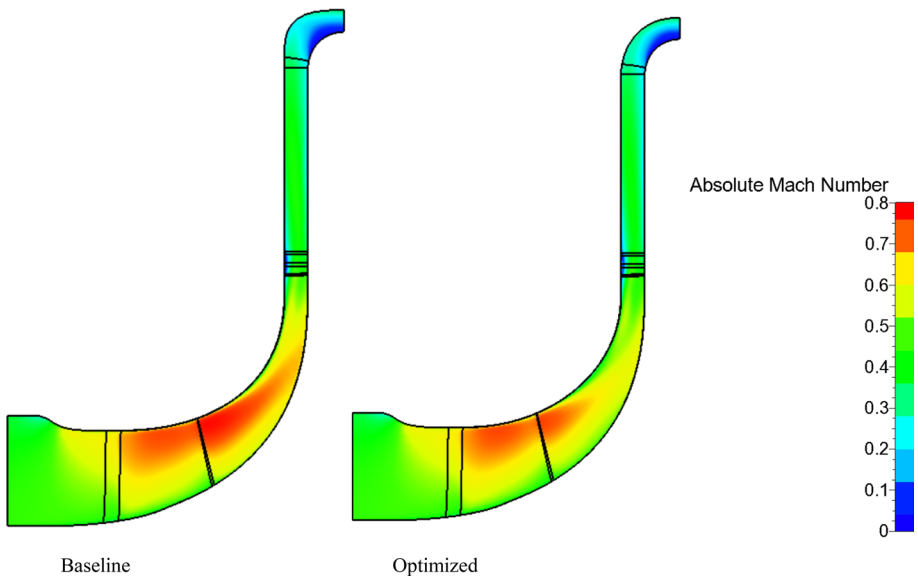

Fig. 22 Absolute Mach number contours of both baseline and optimized geometry

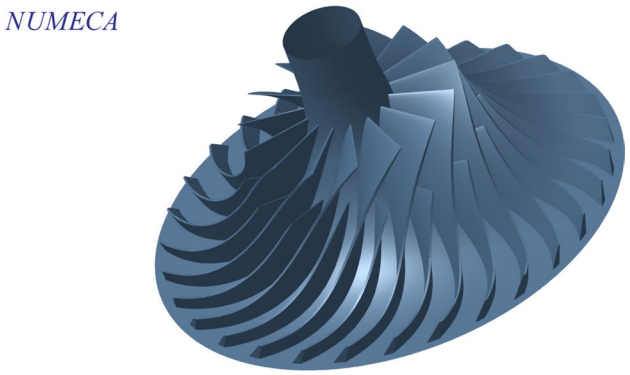

Fig. 23 Optimized 3D Impeller

losses. Unfortunately, we are not able to reduce the tip gap due to the impeller creep. The parametric influence on the global objective is also deliberated through which one can get a good insight into developing an improved centrifugal compressor. This kind of optimization approach reduces the cycle time required for product development thereby reducing the cost involved. This algorithm can be helpful to design engineers in developing new and improved compressor designs.

Declarations

interest statements There is no details for funding and authors disclose no conflict of interest.

References

1. Lakshminarayana B (1996) Fluid dynamics and heat transfer of turbomachinery. Wiley, New York
2. Menter FR (2009) Review of the shear-stress transport turbulence model experience from an industrial perspective. Int J Comput Fluid Dyn 23(4):305–316
3. Trigg MA, Tubby GR, Sheard AG (1999) Automatic genetic optimization approach to two-dimensional blade profile design for steam turbines. J Turbomach 121:11–17
4. Wahba WA, Tourlidakis A (2001) A genetic algorithm to the design of blade profiles for centrifugal pump impellers. AIAA Paper 8:2001–2582
5. Pierret S, Van Den Braembussche RA (1999) Turbomachinery blade design using a navier-stokes solver and artificial neural network. J Turbomach 121:326–332
6. Ahn C-S, Kim K-Y (2003) Aerodynamic design optimization of a compressor rotor with Navier—Stokes analysis. Proceed Instit Mech Eng, Part A: J Power Energy 217(2):179–183. https://doi.org/10.1243/09576500360611209
7. Jang CM, Kim KY (2005) Optimization of a stator blade using response surface method in a single-stage transonic axial compressor. Proceed Instit Mech Eng, Part A, J Power Energy 219(8):595–603
8. Samad A, Kim KY (2009) Application of surrogate modeling to design of a compressor blade to optimize stacking and thickness. Int J Fluid Mach Syst 2(1):1–12
9. Bonaiuti D, Arnone A, Ermini M (2006) Analysis and optimization of transonic centrifugal compressor impellers using the design of experiments technique. J Turbomach 128:786–797
10. D. Bonaiuti and V. Pediroda, (2001) "Aerodynamic Optimization of an Industrial Centrifugal Compressor Impeller Using Genetic Algorithms". Proceed Eurogen
11. R Cosentino, Z Alsalihi, RA Van Den Braembussche "Expert System for Radial Impeller Optimization", Proc., Fourth European Conference on Turbomachinery, Paper No. ATI-CST-039/01
12. Benini E (2004) Three-dimensional multi-objective design optimization of a transonic compressor rotor. J Propuls Power 20(3):204–225
13. A Huppertz, P Flassig, RJ Flassig, M Swoboda (2007) "Knowledge-Based 2D Blade design using multi-objective aerodynamic optimization and a neural network". ASME turbo expo 2007, Montreal, Canada, GT2007–28204
14. Rai MM, Madyavan NK (2000) Aerodynamic Design Using Neural Networks. AIAA J 38(1):173–182
15. Meireles MRG, Almeida PEM, Simoes MG (2003) A comprehensive review for industrial applicability of artificial neural networks. IEEE Trans Industr Electron 50(3):585–601
16. Forrester AIJ, Keane AJ (2009) Recent advances in surrogate-based optimization. Prog Aerospace Sci 7(1):50–79
17. Queipoa NV, Haftka RT, Shyy W, Goel T, Vaidyanathan R, Tucker PK (2005) Surrogate-based analysis, and optimization. Prog Aerospace Sci 8:1–28
18. Bishop CM (1995) Neural networks for pattern recognition. Oxford University Press, Oxford
19. Deb K (2000) An efficient constraint handling method for genetic algorithms. Comput Methods Appl Mech Eng 186:311–338
20. Choi Kim JH, Kim JH (2010) KY Surrogate modeling for optimization of a centrifugal compressor impeller. Int J Fluid Mach Syst 3:29–38
21. K. Rasheed, GADO (1998) "A genetic algorithm for continuous design optimization". PhD thesis, Rutger, State University of New Jersey; New Jersey